

The Pennsylvania State University
APPLIED RESEARCH LABORATORY
Post Office Box 30
State College, PA 16804

**Application of Frequency Domain
Substructure Synthesis Technique for
Plates loaded with Complex Attachments**

by

R. L. Campbell and S. A. Hambric

Technical Report 04-004
April 2004

E. G. Liszka, Director
Applied Research Laboratory

Approved for public release, distribution unlimited

REPORT DOCUMENTATION PAGE				Form Approved OMB No. 0704-0188	
Public reporting burden for this collection of information is estimated to average 1 hour per response, including the time for reviewing instructions, searching existing data sources, gathering and maintaining the data needed, and completing and reviewing this collection of information. Send comments regarding this burden estimate or any other aspect of this collection of information, including suggestions for reducing this burden to Department of Defense, Washington Headquarters Services, Directorate for Information Operations and Reports (0704-0188), 1215 Jefferson Davis Highway, Suite 1204, Arlington, VA 22202-4302. Respondents should be aware that notwithstanding any other provision of law, no person shall be subject to any penalty for failing to comply with a collection of information if it does not display a currently valid OMB control number. PLEASE DO NOT RETURN YOUR FORM TO THE ABOVE ADDRESS.					
1. REPORT DATE (DD-MM-YYYY) 04-2004		2. REPORT TYPE Technical Report		3. DATES COVERED (From - To)	
4. TITLE AND SUBTITLE Application of Frequency Domain Substructure Synthesis Technique for Plates Loaded with Complex Attachments				5a. CONTRACT NUMBER PL01000100	
				5b. GRANT NUMBER	
				5c. PROGRAM ELEMENT NUMBER	
6. AUTHOR(S) R. L. Campbell and S. A. Hambric				5d. PROJECT NUMBER	
				5e. TASK NUMBER	
				5f. WORK UNIT NUMBER	
7. PERFORMING ORGANIZATION NAME(S) AND ADDRESS(ES) Applied Research Laboratory Post Office Box 30 State College, PA 16804				8. PERFORMING ORGANIZATION REPORT NUMBER TR 04-004	
9. SPONSORING / MONITORING AGENCY NAME(S) AND ADDRESS(ES)				10. SPONSOR/MONITOR'S ACRONYM(S)	
				11. SPONSOR/MONITOR'S REPORT NUMBER(S)	
12. DISTRIBUTION / AVAILABILITY STATEMENT Approved for public release, Distribution unlimited					
13. SUPPLEMENTARY NOTES					
14. ABSTRACT The generalized frequency domain substructure synthesis technique proposed by Jetmundsen <i>et al.</i> * has been used to predict the combined response of a bare, edge-stiffened plate and two electronic components. This technique offers a substantial advantage over other coupling techniques because it is uniquely suited to handle data sets of varying origin. Of particular interest is the combination of numerically and experimentally derived frequency response data, which is useful for a structural model comprised of components too complex to model using the finite element method. Limitations of the frequency domain techniques are identified and discussed along with potential methods for avoiding these shortcomings. The synthesis results for the plate and equipment show similar shifts in resonance frequency locations and amplitudes relative to the experimental results for the combined structures. *Jetmundsen, B., Bielawa, R. L., Flannelly, W. G., "Generalized Frequency Domain Substructure Synthesis," <i>Journal of the American Helicopter Society</i> , 1988, pp. 55-64.					
15. SUBJECT TERMS					
16. SECURITY CLASSIFICATION OF:			17. LIMITATION OF ABSTRACT Unclassified Unlimited-UU	18. NUMBER OF PAGES 22	19a. NAME OF RESPONSIBLE PERSON
a. REPORT UNCLASSIFIED	b. ABSTRACT UNCLASSIFIED	c. THIS PAGE UNCLASSIFIED			19b. TELEPHONE NUMBER (include area code)

TABLE OF CONTENTS

Page Number

1	Introduction.....	1
2	Frequency Domain Impedance Coupling Technique	1
	2.1 Traditional FRF Impedance Coupling Technique	2
	2.2 Generalized FRF Impedance Coupling Technique.....	3
	2.3 Mode Truncation Errors.....	5
	2.4 Errors Caused by Rotational Degree of Freedom Truncation	8
3	Synthesis of Plate and Attachment Response	11
4	Summary and Conclusions	16
5	References.....	17

LIST OF FIGURES

Figure Number	Title	Page Number
1.1.	Edge-stiffened plate with complex attachments.	1
2.1.	Coordinate system used for the definition of the mobility matrix.....	2
2.2.	Frequency domain substructure synthesis diagram.	4
2.3.	Modal summation study showing mode truncation effects.	6
2.4.	Beam structure example problem.	7
2.5.	Synthesis example showing effect of mode truncation.	7
2.6.	Choices of interface DOFs to mitigate effects of not including RDOF mobilities: (a) interface DOFs may adequately capture rotational effects, and (b) collinear DOF placement may require RDOF mobilities.	8
2.7.	Plate example for rotational DOF truncation.....	9
2.8.	Results for plate model showing effect of RDOF.	9
2.9.	Translational mobility measurements for the finite difference RDOF approximation.	10
3.1.	Edge-stiffened plate resting on bubble wrap.	11
3.2.	Attached equipment showing the mobility measurement locations: (a) the DC Fan and (b) the switching power supply.....	11
3.3.	Mean measured and predicted admittances for the bare, edge-stiffened plate.	12
3.4.	Mean measured and modified numerical admittances for the bare, edge-stiffened plate.....	13
3.5.	DC fan mobility matrix components (referenced to the grid numbers shown in Figure 3.2a).....	14
3.6.	Switching power supply mobility matrix components (referenced to the grid numbers shown in Figure 3.2b).	15
3.7.	Measured and predicted bare plate and combined plate and equipment admittances.	16

LIST OF TABLES

Table Number	Title	Page Number
2.1.	First and Second order finite difference transformation matrices.	10

LIST OF SYMBOLS

F = force

H = frequency response function

K = stiffness matrix

M = mass or a Boolean mapping matrix

T = transformation matrix

Y = mobility

Z = impedance

p = load vector or modal participation factor

s = linear spacing

u = displacement vector

x = translational coordinate

y = translational coordinate

z = translational coordinate

α = rotational coordinate

β = rotational coordinate

γ = rotational coordinate

η = mechanical loss factor

ω = circular frequency

1 Introduction

Frequency domain substructure synthesis is a modeling technique that enables the prediction of a combined response of individual structures using experimentally measured or numerically predicted frequency response functions (FRFs). The traditional synthesis algorithm [1,2] operates on component impedances and thus generally requires several matrix inversions. An improved algorithm, developed by Jetmundsen *et al.* [3], requires a single matrix inversion with a completely arbitrary interface definition that can easily incorporate connection impedances. The main limitations of the method are the large data requirements and sensitivity to data truncation.

The utility of this technique is demonstrated through a comparison of synthesized and measured admittances of an edge-stiffened plate with attached equipment (see Figure 1.1). The plate mobilities are obtained from a numerical analysis because of the ability to accurately model this structure using a finite element representation. The attachments are characterized experimentally because of their complexity. The following sections describe the synthesis technique and show numerical and experimental results for the plate and equipment.

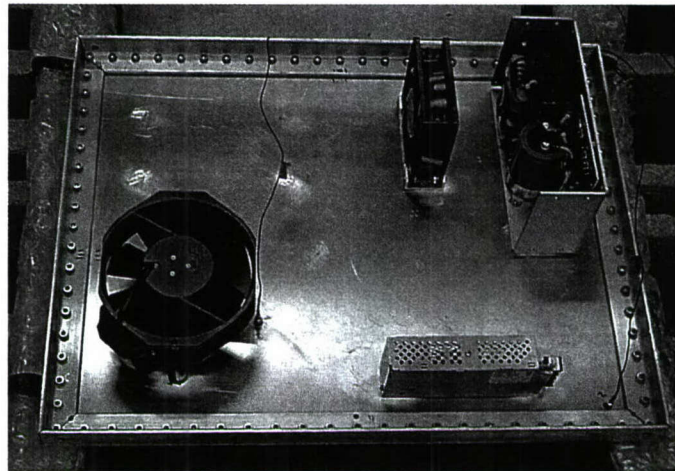


Figure 1.1. Edge-stiffened plate with complex attachments.

2 Frequency Domain Impedance Coupling Technique

The frequency domain impedance coupling technique represents a method to predict the response of a structure using substructure dynamic information. Other substructure analysis techniques are available and are commonly used. Of these, the most popular are finite element substructuring [1,4] and component modes synthesis [1,2]. Finite element substructuring combines structural models of individual structures through reduced representations of the matrices, while component modes synthesis combines substructure eigenvectors to compute eigenvectors and eigenvalues of the combined structure. Often, component modes synthesis is used in a finite element substructure analysis to improve the accuracy of dynamic predictions. Both techniques are well suited for numerical analyses where the mass and stiffness matrices can be defined, but may have significant shortcomings when dealing with experimental data. The frequency domain impedance coupling technique can be used for numerical, experimental, or a

combination of these because the technique is based on component mobilities which can be directly measured or numerically computed.

2.1 Traditional FRF Impedance Coupling Technique

Impedance coupling via frequency response functions requires knowledge of the mobility matrices, Y , for each of the substructures being combined. A mobility matrix represents the inverse of an impedance matrix ($Y = Z^{-1}$, where Z is the structural impedance), which is defined as follows:

$$\{p\} = [Z] \cdot \{\dot{x}\}, \quad (1)$$

where $\{p\}$ is the load vector and $\{\dot{x}\}$ is the velocity vector.

In general, the mobility matrices are $6N \times 6N$ complex-valued matrices, where N is the number of nodes. The mobility matrix for a single node is:

$$\begin{Bmatrix} \dot{x} \\ \dot{y} \\ \dot{z} \\ \dot{\alpha} \\ \dot{\beta} \\ \dot{\gamma} \end{Bmatrix} = \begin{bmatrix} Y_{xx} & Y_{xy} & Y_{xz} & Y_{x\alpha} & Y_{x\beta} & Y_{x\gamma} \\ Y_{yx} & Y_{yy} & Y_{yz} & Y_{y\alpha} & Y_{y\beta} & Y_{y\gamma} \\ Y_{zx} & Y_{zy} & Y_{zz} & Y_{z\alpha} & Y_{z\beta} & Y_{z\gamma} \\ Y_{\alpha x} & Y_{\alpha y} & Y_{\alpha z} & Y_{\alpha\alpha} & Y_{\alpha\beta} & Y_{\alpha\gamma} \\ Y_{\beta x} & Y_{\beta y} & Y_{\beta z} & Y_{\beta\alpha} & Y_{\beta\beta} & Y_{\beta\gamma} \\ Y_{\gamma x} & Y_{\gamma y} & Y_{\gamma z} & Y_{\gamma\alpha} & Y_{\gamma\beta} & Y_{\gamma\gamma} \end{bmatrix} \cdot \begin{Bmatrix} F_x \\ F_y \\ F_z \\ M_x \\ M_y \\ M_z \end{Bmatrix}, \quad (2)$$

where the coordinates are defined in Figure 2.1. As shown in Equation 2, 75% of the components in the mobility matrix involve a rotational coordinate, an important detail that is discussed later.

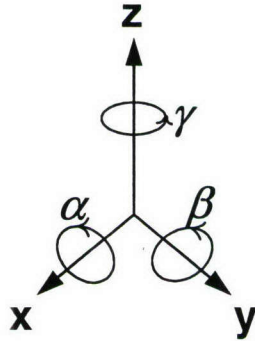


Figure 2.1. Coordinate system used for the definition of the mobility matrix.

Mobility matrices similar to the matrix shown in Equation 2 can be defined for all nodes of each structure that is to be coupled. Furthermore, these matrices can be partitioned according to the internal (i) and coupling (c) DOFs. The partitioned mobility matrices for two substructures, A and B , for frequency ω are:

$$Y^A(\omega) = \begin{bmatrix} Y_{ii}^A & Y_{ic}^A \\ Y_{ci}^A & Y_{cc}^A \end{bmatrix} \quad (3)$$

$$Y^B(\omega) = \begin{bmatrix} Y_{ii}^B & Y_{ic}^B \\ Y_{ci}^B & Y_{cc}^B \end{bmatrix}. \quad (4)$$

The classical derivation of the FRF substructure synthesis technique employs impedance matrices instead of mobility matrices [1,2]. With these and compatibility of displacements and force equilibrium at the coupling DOFs:

$$\begin{aligned} u_c^A &= u_c^B \\ F_c^A + F_c^B &= F_c \end{aligned} \quad (5)$$

the following relation for the coupling of substructures A and B can be derived (see Reference 2 for a complete derivation):

$$Y^* = \begin{bmatrix} Z_{ii}^A & Z_{ic}^A & 0 \\ Z_{ci}^A & Z_{cc}^A + Z_{cc}^B & Z_{ci}^B \\ 0 & Z_{ic}^B & Z_{ii}^B \end{bmatrix}^{-1}, \quad (6)$$

where Y^* is the mobility matrix for the coupled system. As seen in this relation (for two structures), such a coupling process requires three matrix inversions: one to obtain the impedance matrix of substructure A from a measured or predicted mobility matrix, one for the substructure B mobility matrix, and a third inversion for assembled impedance matrix to obtain the mobility. In general, the number of matrix inversions is one greater than the number of substructures being combined. The size of these matrices are $n_A \times n_A$ for substructure A , $n_B \times n_B$ for substructure B , and $n^* \times n^*$ for the combined structure, where $n^* = n_A + n_B - n_C$. It is also apparent from Equation 6 that point and cross mobilities (or impedances) are required **for all DOFs and all frequencies** involved in the analysis. It is this fact that often limits the usefulness of the impedance coupling technique.

2.2 Generalized FRF Impedance Coupling Technique

The large computation requirements of the traditional impedance coupling technique (shown in Equation 6) can be avoided by using the generalized approach developed by Jetmundsen *et al.* [3,5]. The formulation for two substructures, A and B , is (see Reference 5 for a derivation):

$$Y^* = \begin{bmatrix} Y_{ii}^A & Y_{ic}^A & 0 \\ Y_{ci}^A & Y_{cc}^A & Y_{ci}^B \\ 0 & Y_{ic}^B & Y_{cc}^B \end{bmatrix} - \begin{bmatrix} Y_{ic}^A \\ Y_{cc}^A \\ Y_{ic}^B \end{bmatrix} \left[Y_{cc}^A + Y_{cc}^B \right]^{-1} \begin{bmatrix} Y_{ic}^A \\ Y_{cc}^A \\ Y_{ic}^B \end{bmatrix}^T. \quad (7)$$

It is apparent from Equation 7 that only a single matrix inversion of size $n_C \times n_C$ is required for this coupling algorithm, which is a significant improvement over the traditional approach. The theory has been generalized to incorporate Boolean mapping matrices, called connectivity matrices, that define the structural interconnections [5]. The generalized relation is:

$$Y^* = Y_{\alpha\alpha} - [M \otimes Y_{\alpha\gamma}] \cdot \left[\sum_{q=1}^N M_q^T M_q \otimes Y_{\gamma\gamma}^q \right]^{-1} \cdot [M \otimes Y_{\alpha\gamma}]^T, \quad (8)$$

where M is the Boolean mapping matrix defining the interfacial sign convention for the coupling forces and their reactions, α is a substructure identifier in addition to a set of internal DOFs, γ is an interface identifier that implies an interface DOF set, \otimes represents a matrix element-by-element multiplication, and N is the number of substructures. The notation is best understood with the use of an example.

Consider the structure shown in Figure 2.2, which consists of three substructures— A , B , and C —and three interfaces— I , J , and K . Each column of the mapping matrix corresponds to an interface, while each row corresponds to a substructure. A positive direction is arbitrarily assigned to each interface, as shown by the positive and negative signs adjacent to the interface arrows in Figure 2.2. The arbitrary sign convention is applied to the interfaces for the purpose of constructing the mapping matrix. For each substructure (i.e., each row of the matrix), a “+1” or “-1” is placed in the columns corresponding to an interface that connects to the substructure. The decision to use a “+1” or “-1” is based upon the chosen sign convention. The mapping matrix corresponding to the structure in Figure 2.2 is:

$$M = \begin{array}{ccc|c} & I & J & K \\ \hline A & 1 & -1 & 0 \\ B & -1 & 0 & 1 \\ C & 0 & 1 & -1 \end{array} \quad (9)$$

The mobility matrix, $Y_{\alpha\alpha}$, is defined as:

$$Y_{\alpha\alpha} = \begin{bmatrix} Y_{aa}^A & 0 & 0 \\ 0 & Y_{bb}^B & 0 \\ 0 & 0 & Y_{cc}^C \end{bmatrix}, \quad (10)$$

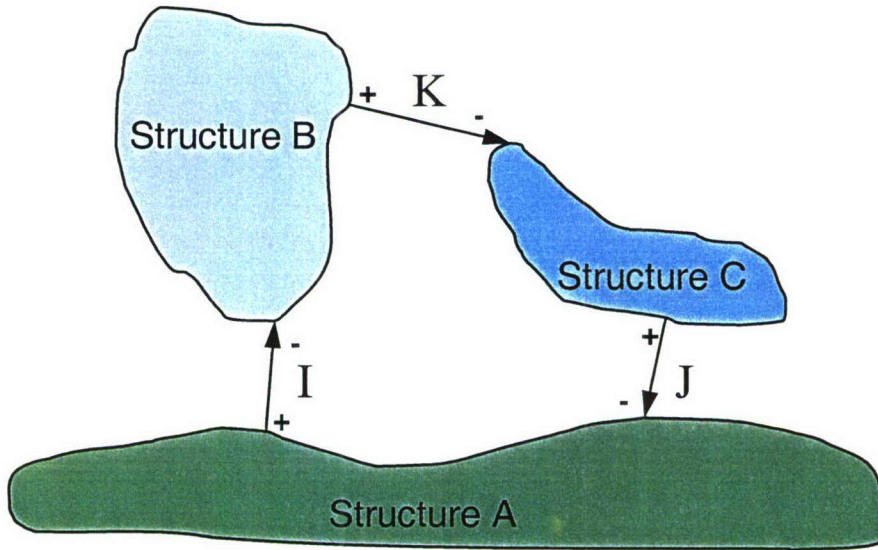


Figure 2.2. Frequency domain substructure synthesis diagram.

where a represents the internal degrees of freedom for substructure A , b are the internal degrees of freedom for substructure B , and so on. These DOF sets are the DOFs for which mobility information will be computed in the synthesized mobility matrix. If response information is required for any of the interface degrees of freedom, they can be combined in these DOF sets. However, each interface DOF can only reside in one set. For instance, if results are required for the interface DOFs associated with the I interface, these DOFs can be included in either the a or the b set, but not both. Note that the order of the DOF sets in $\alpha = \{a, b, c\}$ correspond to the order of the substructures in the rows of the mapping matrix (Equation 9). The cross mobility matrix between interface and internal DOFs is defined as:

$$Y_{\alpha\gamma} = \begin{bmatrix} Y_{ai}^A & Y_{aj}^A & Y_{ak}^A \\ Y_{bi}^B & Y_{bj}^B & Y_{bk}^B \\ Y_{ci}^C & Y_{cj}^C & Y_{ck}^C \end{bmatrix}. \quad (11)$$

Here, the i, j , and k DOF sets represent the DOFs associated with the I, J , and K , interfaces, respectively. The order of the interface DOF sets, $\gamma = \{i, j, k\}$, corresponds to the columns of the mapping matrix. When multiplied by the mapping matrix, M , using an element by element multiplication, some of the components in this matrix are nullified (e.g., Y_{ak}^A becomes zero because the K interface does not involve the A substructure):

$$M \otimes Y_{\alpha\gamma} = \begin{bmatrix} 1 & -1 & 0 \\ -1 & 0 & 1 \\ 0 & 1 & -1 \end{bmatrix} \otimes \begin{bmatrix} Y_{ai}^A & Y_{aj}^A & Y_{ak}^A \\ Y_{bi}^B & Y_{bj}^B & Y_{bk}^B \\ Y_{ci}^C & Y_{cj}^C & Y_{ck}^C \end{bmatrix} = \begin{bmatrix} Y_{ai}^A & -Y_{aj}^A & 0 \\ -Y_{bi}^B & 0 & Y_{bk}^B \\ 0 & Y_{cj}^C & -Y_{ck}^C \end{bmatrix}. \quad (12)$$

The final part of Equation 8 that requires explanation is the summation term:

$$\sum_{q=1}^N M_q^T M_q \otimes Y_{\gamma\gamma}^q. \quad (13)$$

Here, a subscript of the mapping matrix represents a row of the matrix. For this example, $M_1 = [1 \ -1 \ 0]$. The summation from $q = 1$ to N is a summation over all substructures, where the order corresponds to the rows of the mapping matrix (e.g., $q = 1$ is the first row of M which corresponds to substructure A , $q = 2$ is the second row of M which corresponds to substructure B , and so on). With this definition, we have $Y_{\gamma\gamma}^1 = Y_{\gamma\gamma}^A$ where γ is the internal DOF set previously defined.

While the theory for performing substructure synthesis analyses is exact, the accuracy is often limited by incompleteness or inaccuracies of the mobility matrices. These deficiencies can be a result of numerous sources. The major sources, however, are often a result of mode truncation or lack of rotational degrees of freedom (RDOFs). Both of these sources of error are discussed next.

2.3 Mode Truncation Errors

Mode truncation errors are a result of generating frequency response functions from an incomplete modal database. This modal database can be derived from either a numerical model or experimental measurements. In any case, the errors result from using only a partial set of

eigenvectors in a modal summation solution for a system's response. For example, a finite element model may consist of N DOFs from which N mode shapes can be derived. However, due to practical limitations, usually only the first M modes are retained ($M < N$). Such a truncation generally has a negligible effect on the response at resonance frequencies, but does shift the antiresonances *upward* in frequency. (The reason for the upward shift in antiresonance frequency can be explained by considering the residual term that is discussed later.) While this effect may have a negligible impact on most applications of the FRFs, substructure synthesis methods can be particularly sensitive to it [2,6].

The effect of mode truncation is shown in the plots of Figure 2.3. This figure shows results from modal summation solutions for a cantilever beam finite element model (structure 0 in Figure 2.4). The figure indicates the increasing errors at the antiresonance locations associated with the drive point FRF near the tip of the beam as the number of summed modes decreases from $N = M = 42$ to $M = 15 < N$. The consequence of these errors is often minimal for applications where the system response near the resonances is of concern. However, for frequency response function coupling, errors in the FRFs at all frequencies may impact the coupled response. This is demonstrated by synthesizing the response of the beam structure of Figure 2.4 using the component responses computed as follows: structure 0 response computed using a direct frequency response analysis (equivalent to a modal summation solution using all modes); structure 0 response using a modal summation with modes to 10 kHz; structure 0 response computed using a modal summation with modes 10 kHz and a residual vector to account for the truncated modes (residual vectors are discussed below). A direct frequency response analysis was used in all cases for structures 1 and 2. The drive point FRFs at grid 7 for the combined structure are shown in Figure 2.5. This figure shows excellent agreement between the synthesized responses for all cases except the case using a modal summation and no residual vector, wherein differences exist in both the resonance and antiresonance frequencies. Based on these results, it is important for synthesized results that errors associated with modal truncation be minimized whenever possible.

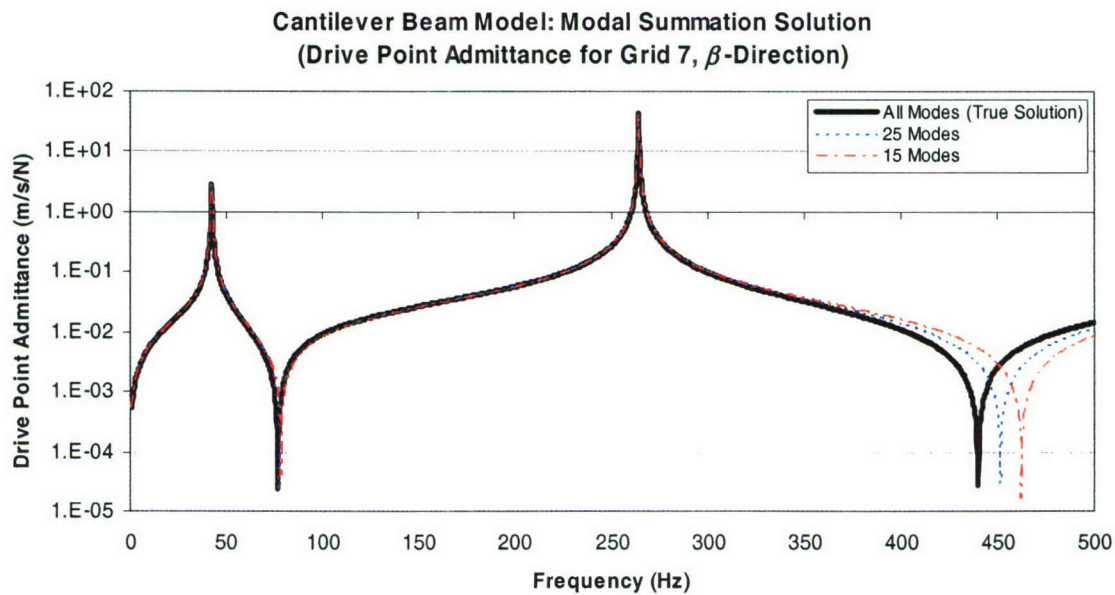


Figure 2.3. Modal summation study showing mode truncation effects.

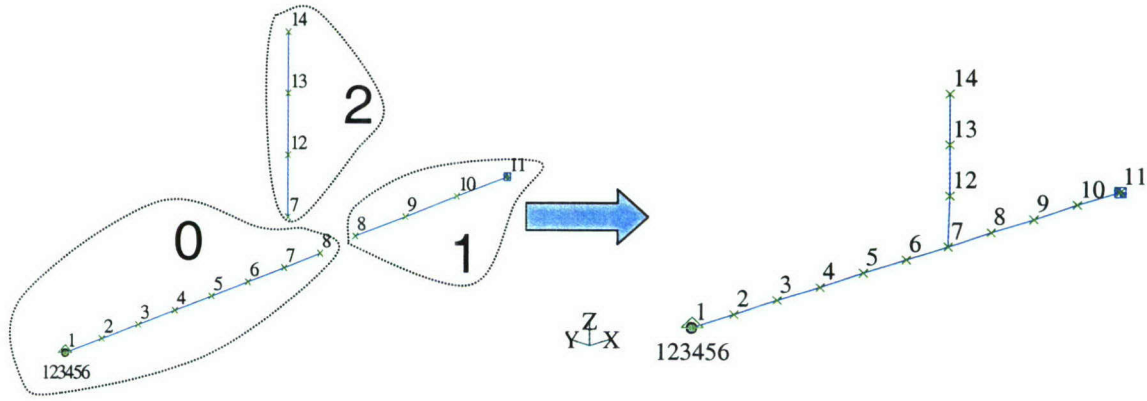


Figure 2.4. Beam structure example problem.

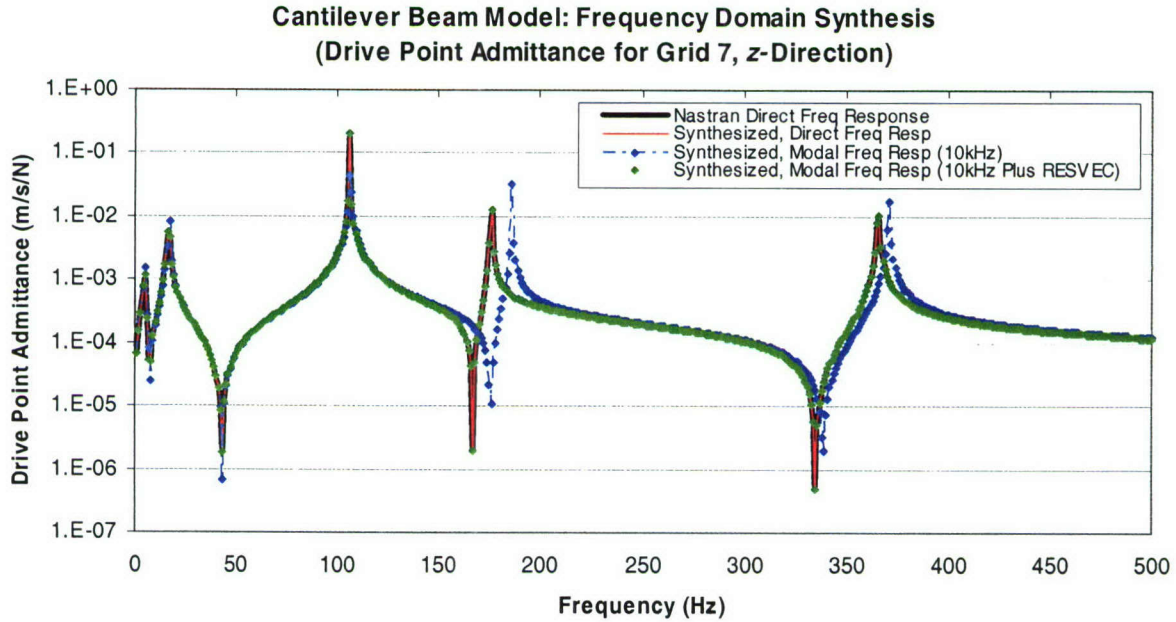


Figure 2.5. Synthesis example showing effect of mode truncation.

Because it is often not practical to use all possible mode shapes in such a solution due to memory limitations for numerical modes or measurement limitations for experimental modes, the effect of the truncated modes can be approximated with the use of *residuals* [2]. Both ‘low-frequency’ and ‘high-frequency’ mode truncation can be accounted for using residuals. The truncated low-frequency modes exhibit a mass-like behavior while the high-frequency modes exhibit a stiffness-like behavior [2]. If the modal summation is represented in terms of the modal parameters (resonance frequencies (ω_r), damping (η_r), and modal constants ($r^{A_{jk}}$) for a general mobility between points j and k), the modal summation has the following form:

$$Y_{jk}(\omega) = -\frac{i}{\omega M_{jk}^R} + \sum_{r=m_1}^{m_2} \frac{i\omega r^{A_{jk}}}{\omega_r^2 - \omega^2 + i\eta_r \omega_r^2} + \frac{i\omega}{K_{jk}^R}, \quad (14)$$

where M_{jk}^R is the residual mass, K_{jk}^R is the residual stiffness, and m_1 and m_2 are the summation limits, where m_1 indicates truncation of low order modes and $m_2 - m_1 + 1$ is the total number of modes used in the summation. M_{jk}^R and K_{jk}^R are dependent on the applied loading, and methods to estimate their values may be found in Reference 2. Commercial finite element solvers also may offer methods to account for the residual terms when performing a modal summation solution. MSC/NASTRAN, for example, can compute a residual vector for each load condition to account for the truncated modes by including the bulk data entry “PARAM,RESVEC,YES” [7]. The process involves a static solution of the model to obtain deflection shapes that are then modified or discarded to make them linearly independent of and orthogonal to the mode shapes. The residual vectors are computed and appended to the mode shape array for use in subsequent modal summation solutions.

2.4 Errors Caused by Rotational Degree of Freedom Truncation

The second major source of error in frequency response function coupling is associated with neglecting components of the mobility matrices. Often the components not included are the mobilities associated with rotational coordinates [8]. As discussed previously, 75% of the complete mobility matrix involves a rotational coordinate. The importance of these mobilities depends on the components being coupled and the interface DOF placement. For example, a structure with a broad interface that is connected using several DOFs, such as the structure shown in Figure 2.6a, may not require the use of the rotational terms because the translational terms inherently provide the rotational information [1]. However, a structure that has point or collinear interface DOFs (see Figure 2.6b) may require all rotational terms or rotational terms about the collinear axis, respectively.

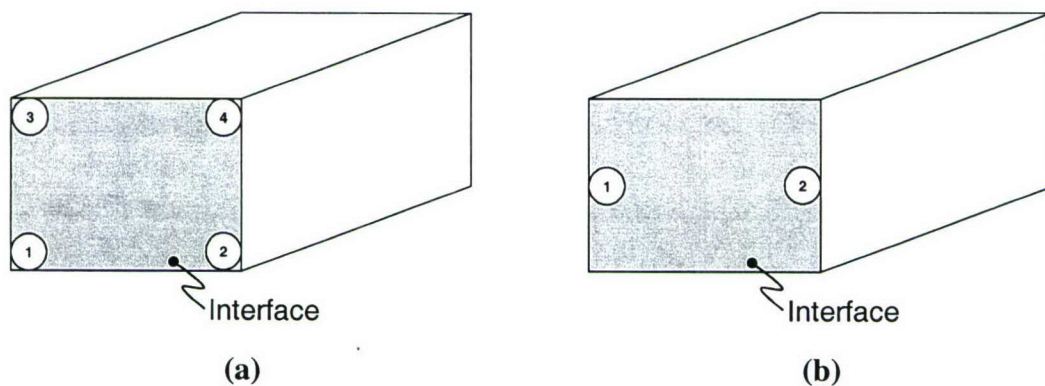


Figure 2.6. Choices of interface DOFs to mitigate effects of not including RDOF mobilities: (a) interface DOFs may adequately capture rotational effects, and (b) collinear DOF placement may require RDOF mobilities.

The need for rotational degrees of freedom is demonstrated using the plate/mass model shown in Figure 2.7. Here, the mass (structure B) is joined to the plate (structure A) at two collinear points on the interface. The combined response is computed in three ways: 1) Nastran solution to the combined model (i.e., the true solution), 2) frequency domain synthesis using translational DOFs (x , y , and z) only, and 3) frequency domain synthesis using DOFs x , y , z , and β . The drive point response at one of the interface grids for each of these cases is shown in

Figure 2.8. This figure shows good agreement between cases 1 and 3 for both resonance frequencies and amplitudes across the entire spectrum. However, the results for case 2 indicate a missed resonance at 155. Hz, incorrect resonance and antiresonance frequencies at several locations (e.g., 410. Hz), and different amplitudes at several frequencies.

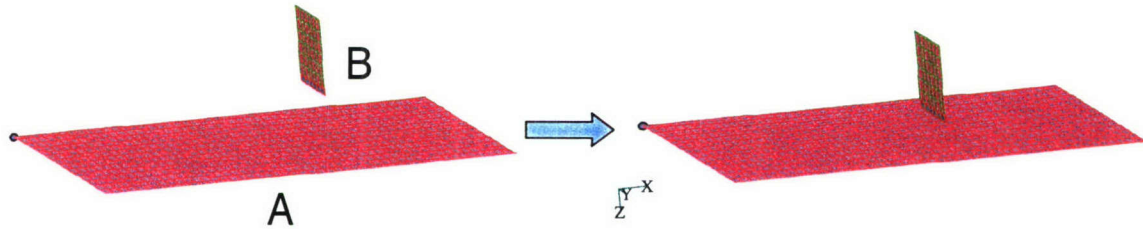


Figure 2.7. Plate example for rotational DOF truncation.

Plate and Mass Model: Effect of Rotational DOFs on Synthesis

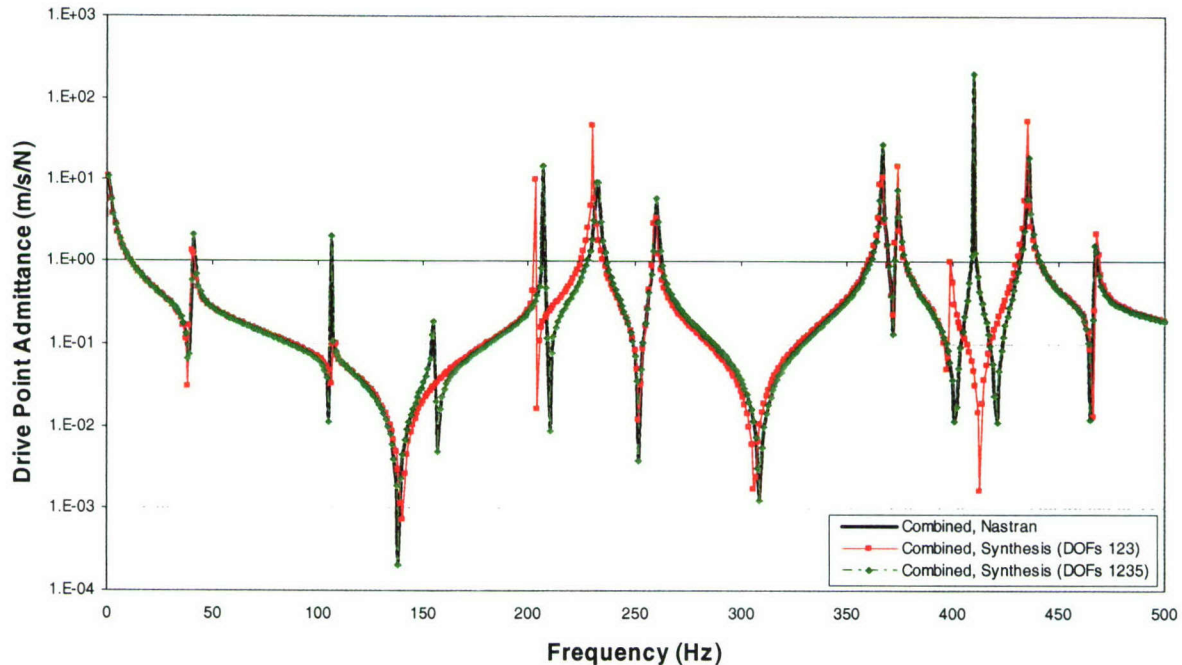


Figure 2.8 Results for plate model showing effect of RDOF.

Rotational DOF mobilities are usually neglected due to the difficulty associated with measuring rotational moments and accelerations at a point. While various attempts have been made to develop an accurate method for measuring these mobilities, the most commonly used approach is to infer the rotational information from measured translational information using a finite difference approach [9]. ANSI S2.34-1984 defines standard methods for measuring or estimating the RDOF mobilities using either translational measurements or rotational measurements involving specialized fixtures [10].

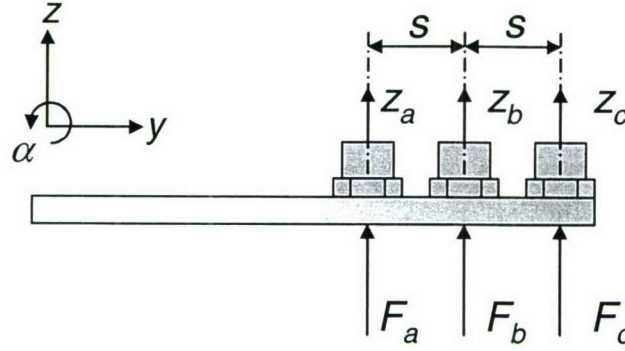


Figure 2.9. Translational mobility measurements for the finite difference RDOF approximation.

The finite difference approach involves the measurement of translational point and cross mobilities as shown in Figure 2.9. The number of required measurements is governed by the desired accuracy of the results. The order of accuracy¹ is one less than the number of measurement points when the traditional finite difference formulae are employed. For example, first order accuracy requires the measurement of mobilities for two locations, second order requires three locations, and so on. A compact implementation of this method has been implemented by Duarte and Ewins [9]. Their method employs the following relation:

$$H_{est} = \begin{bmatrix} H_{zz} & H_{z\alpha} \\ H_{z\alpha}^T & H_{\alpha\alpha} \end{bmatrix} = [T][H_{meas}][T]^T, \quad (15)$$

where H_{meas} is the measured mobility matrix, H_{est} is the estimated mobility matrix containing RDOF terms, and T is the transformation matrix that is defined according to the approximation order. The transformation matrices for first and second order schemes are shown in Table 2.1. These matrices require a constant spacing of the measurement locations similar to the spacing shown in Figure 2.9. The forward and backward differencing schemes shown in this table are required for estimating mobility information near the edges of a structure. Transformation

Table 2.1. First and Second order finite difference transformation matrices.

	First Order	Second Order
Forward	$\begin{bmatrix} 0 & 1 \\ 1/s & -1/s \end{bmatrix}$	$\frac{1}{2s} \begin{bmatrix} 0 & 0 & 2s \\ -1 & 4 & -3 \end{bmatrix}$
Central	N/A	$\frac{1}{2s} \begin{bmatrix} 0 & 2s & 0 \\ -1 & 0 & 1 \end{bmatrix}$
Backward	$\begin{bmatrix} 0 & 1 \\ -1/s & 1/s \end{bmatrix}$	$\frac{1}{2s} \begin{bmatrix} 0 & 0 & 2s \\ 1 & -4 & 3 \end{bmatrix}$

¹ The prediction error is related to the sample spacing as follows: N^{th} order has accuracy on the order of S^N , where S is the sample spacing.

matrices for unequal spacing and approximation orders other than first or second can be developed using the general approach described in Reference 10. Here, the RDOFs and translational mobilities are related in terms of the partial derivatives of the translational mobility at the point of interest. Formulae to approximate the partial derivatives are then developed based on the finite difference approach.

3 Synthesis of Plate and Attachment Response

As stated previously, the frequency domain substructure synthesis technique is aptly suited to accommodate experimental, numerical, or any combination of these data sources. The edge-stiffened plate (see Figure 3.1) with attached electronic equipment (DC fan and switching power supply shown in Figure 3.2) represents a case where a combination of numerical and experimental data is most appropriate. The advantage of using a numerical model over an experimental characterization is mainly due to the large data requirements of the synthesis process. Numerically, the point and cross mobilities are easily acquired through multiple load cases. Acquiring similar data experimentally could require considerable effort. However, depending on the component complexity it may be more effective to experimentally characterize a component rather than invest a significant amount of time developing an accurate model of the

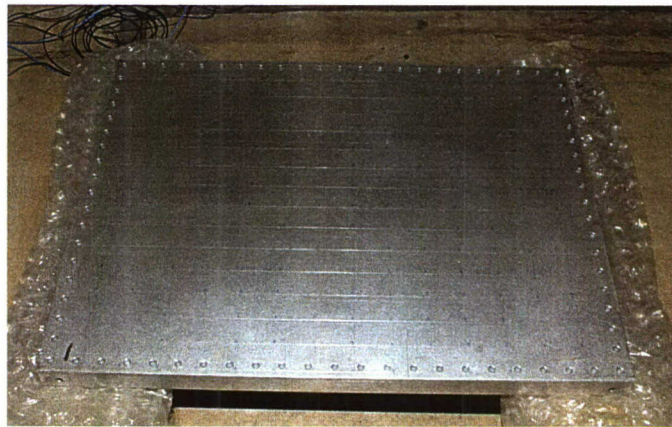


Figure 3.1. Edge-stiffened plate resting on bubble wrap.

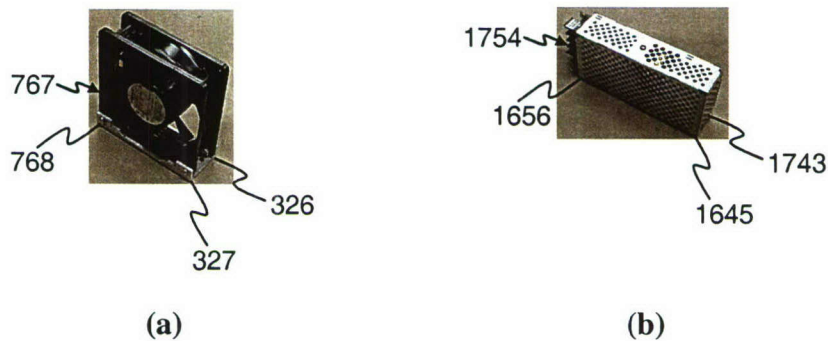


Figure 3.2. Attached equipment showing the mobility measurement locations: (a) the DC Fan and (b) the switching power supply.

structure. The DC fan and switching power supply are two such components that would require significantly more time to model than to experimentally characterize. Based on this, the plate mobilities are determined from a FE model while the attachments are characterized experimentally. A description of the plate, the finite element model of the plate, and the electronic equipment is provided in Reference 11.

Even though the plate has a relatively simple construction, the predicted mobility matrix is slightly different from the measured mobility matrix (mainly due to inaccuracies in the plate/stiffener interface representation in the model). The main differences involve the resonance frequencies and damping levels, as shown by differences in frequency and magnitude of the peaks in the mean surface admittance (see Figure 3.3). Because the performance of the synthesis technique is being investigated here, it is important to tune the plate model to match the experimental results such that the differences associated with modeling errors are minimized. The model was tuned by modifying the computed resonance frequencies and damping to match those determined experimentally. This process involves two steps: 1) an identification step where the numerical and experimental modes are matched based on a modal assurance criteria (MAC) analysis (see Reference 11) between the numerical and experimental results, and 2) an adjustment step where the numerical resonance frequencies and modal damping levels are adjusted to match the experimental results. The result of this process is a model that has a resonant character that accurately represents the dynamic characteristics of the plate up to a frequency of 500 Hz. The mean admittance for the experimental and numerical results due to a common drive point in the normal direction is shown in Figure 3.4. As indicated by this figure,

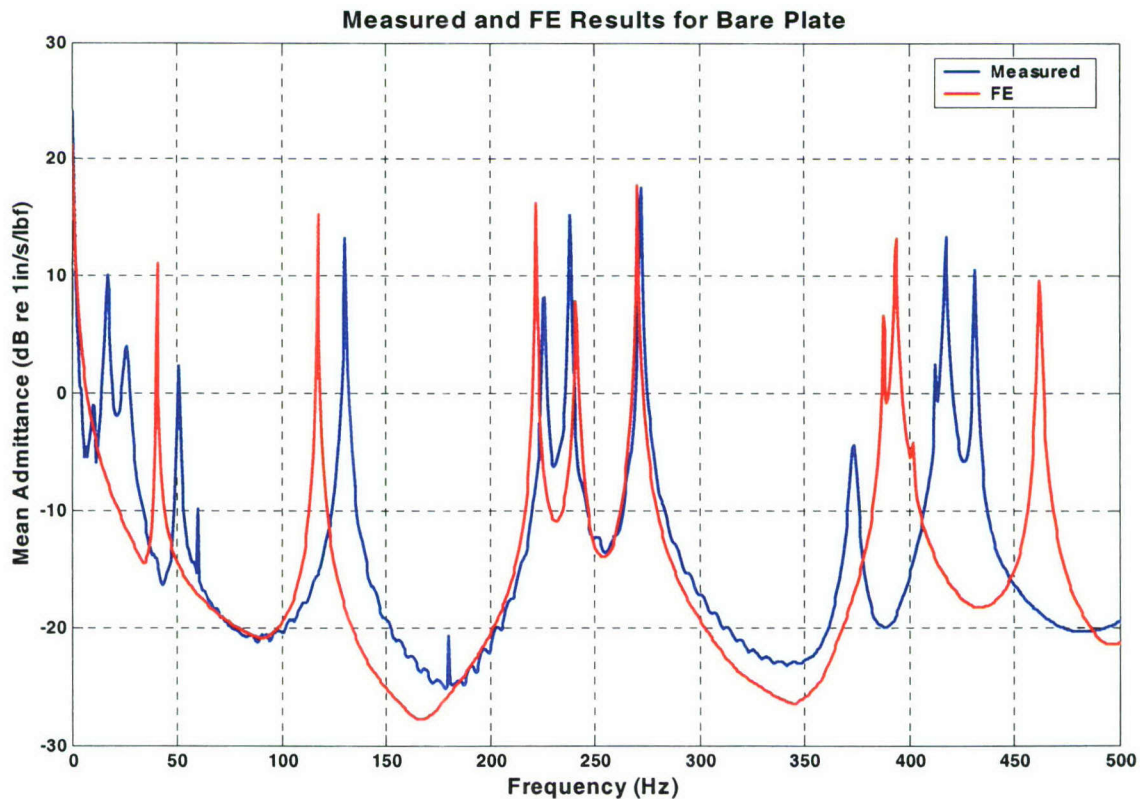


Figure 3.3. Mean measured and predicted admittances for the bare, edge-stiffened plate.

the modified numerical and experimental data sets agree well in terms of resonance frequency location and peak amplitude. Note that the resonances below ~50 Hz are rigid body modes that result from the mass of the plate and the stiffness of the bubble wrap used during testing (see Figure 3.1).

The next step in the analysis is to define the interface degrees of freedom. The narrow attachment surfaces of the equipment prohibited an accurate estimation of rotational degrees of freedom at the attachment points. Therefore, interface points were located at the four corners of each attachment surface to inherently capture the rotational aspects of the structure as previously discussed. In addition, only the translational DOFs normal to the plate surface were used in the analysis because of the difficulty associated with measuring the in-plane mobilities. Because the majority of the plate modes involve out-of-plane motion, excluding the in-plane DOFs should not have a significant impact on the results. The attachment locations are shown in Figure 3.2.

The mobility matrices for the bare plate were obtained by performing a modal frequency response using the modified eigenvalues and damping levels as discussed above. Effects of mode truncation were minimized by using eigenvectors with frequencies up to 4 kHz and MSC/Nastran's residual vector method. Point and cross mobilities for all of the attachment DOFs were obtained through the use of several load cases.

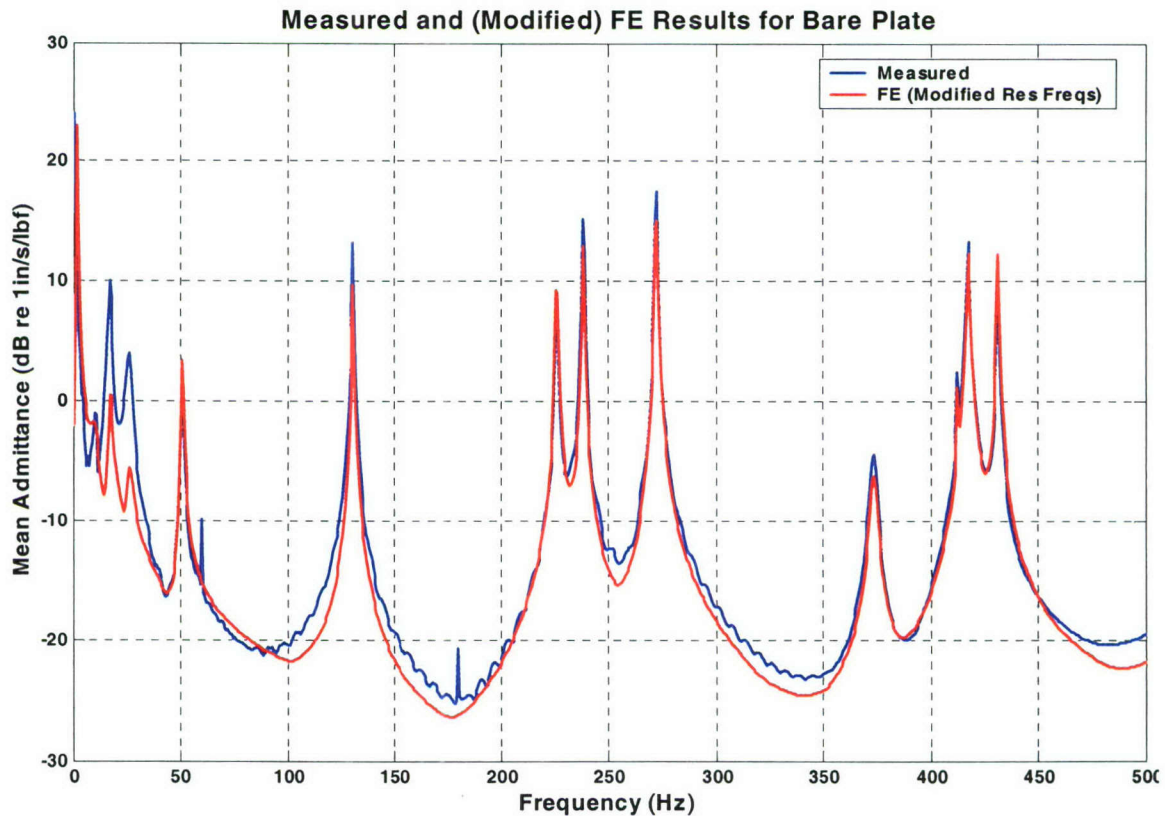


Figure 3.4. Mean measured and modified numerical admittances for the bare, edge-stiffened plate.

The mobility matrices for the attached equipment were obtained experimentally using a tap test (an impact hammer to measure the applied force and accelerometers to measure the response). Results from these measurements for the translational DOFs are shown in Figure 3.5 for the DC fan and in Figure 3.6 for the switching power supply. The plots in these figures show the highly damped equipment mobilities. The impedance coupling technique is a valid candidate for this type of data since an accurate modal model (which is required for other synthesis techniques) would be difficult to derive. It should be noted that the low frequency resonances (approximately less than 50 Hz) shown in these figures are rigid body modes that result from resting the structures on bubble wrap during the testing.

The mobilities of the combined structure are predicted using the measured equipment mobilities and the numerically generated mobilities of the bare plate. The mobilities of the plate

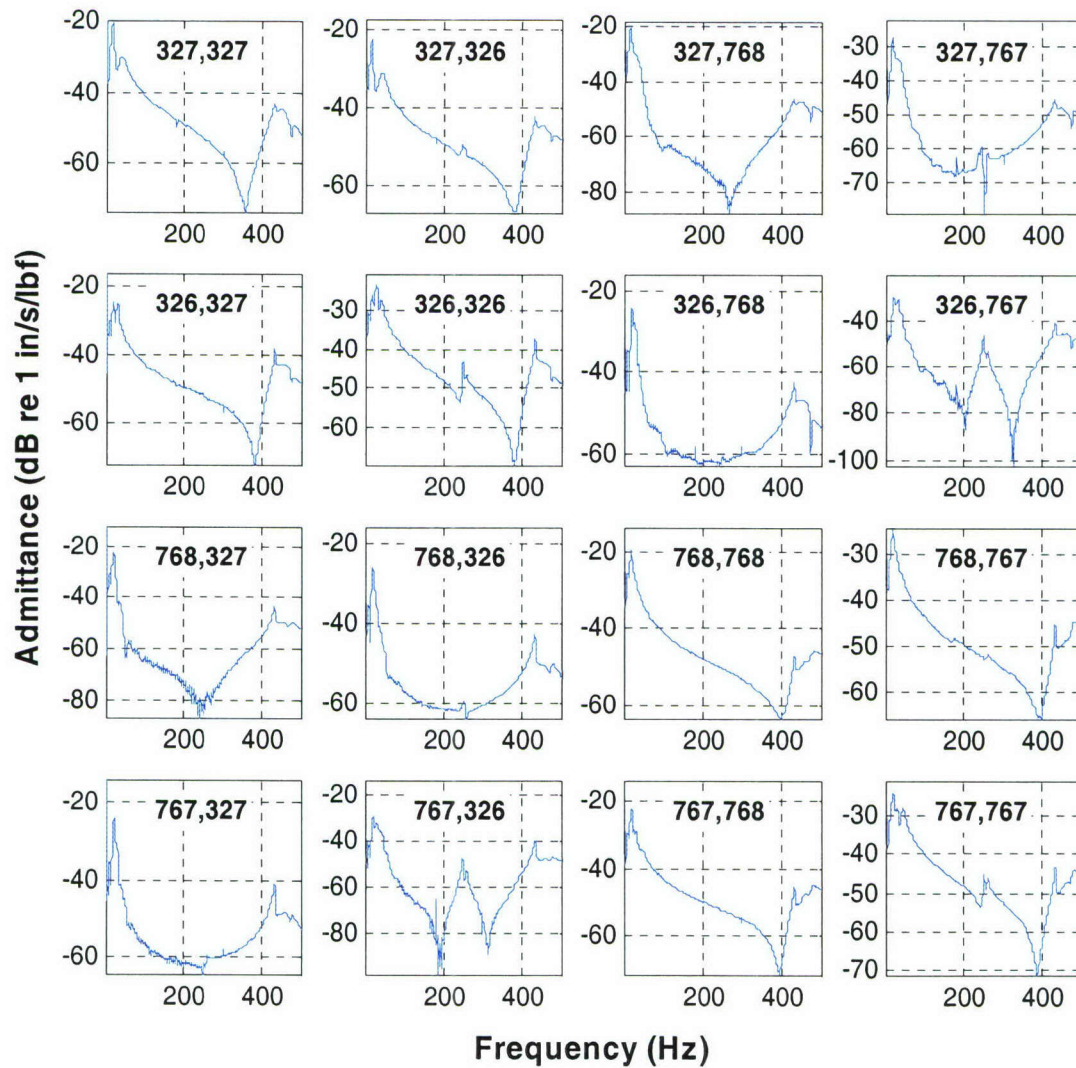


Figure 3.5. DC fan mobility matrix components (referenced to the grid numbers shown in Figure 3.2a).

and attachments are also obtained experimentally. The attachments are joined to the plate using J-B® WELD Kwik Weld adhesive and small flat washers at the four mounting locations of each component to provide point-like attachments. The results of both data sets are provided in Figure 3.7. These results show a similar shift in both resonance frequencies and amplitudes between the bare plate and plate with equipment mobilities. Note that the synthesized results ignore the effect of rotational mobilities and translation for the in-plane directions.

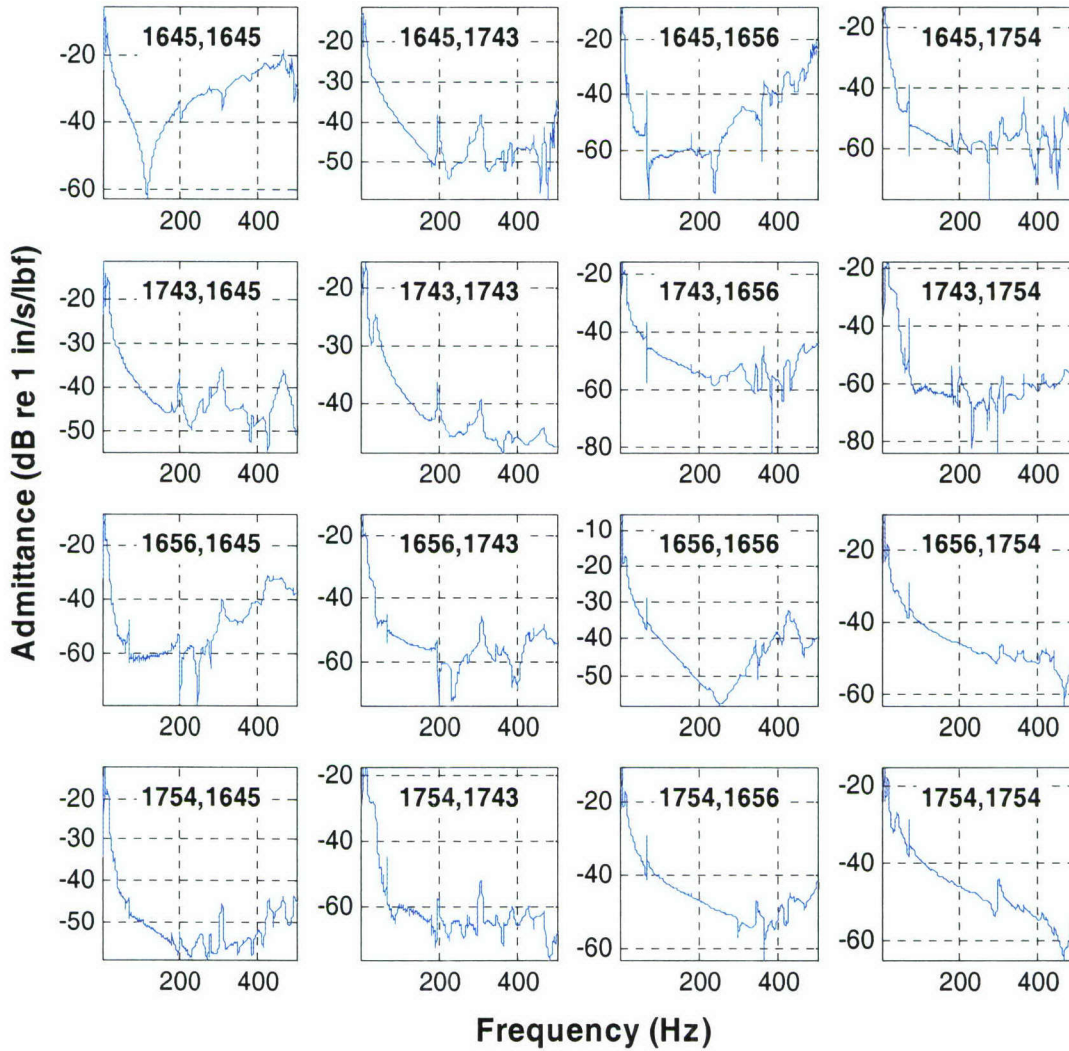


Figure 3.6. Switching power supply mobility matrix components (referenced to the grid numbers shown in Figure 3.2b).

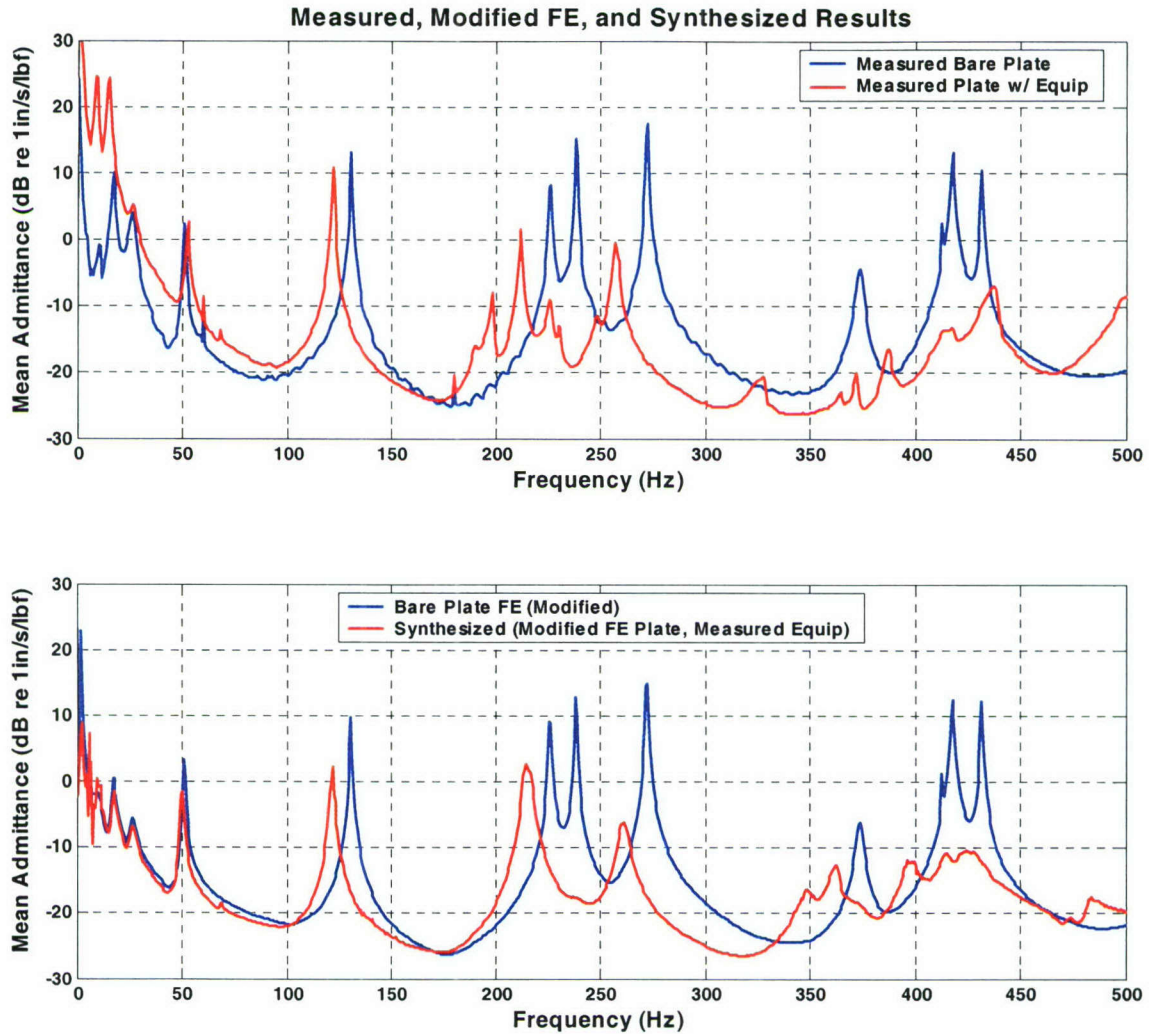


Figure 3.7. Measured and predicted bare plate and combined plate and equipment admittances.

4 Summary and Conclusions

The generalized frequency domain substructure synthesis technique proposed by Jetmundsen *et al.* has been used to compute the combined response of a bare, edge-stiffened plate and two electronic components. The FRF coupling technique was chosen over other coupling methods because it is better suited to combine data sets of varying origin. Furthermore, Jetmundsen's generalized FRF technique has been used because it offers a significant computational improvement over the traditional frequency domain technique. The generalized method is also amenable to interfacial impedances and offers completely arbitrary interface definitions for the combination of multiple substructures.

The major shortcomings of the frequency domain techniques are identified as modal truncation and incomplete mobility matrices. The modal truncation effects are only important when mobilities are acquired from modal summation solutions, and these effects can be

minimized through the inclusion of residual terms. Incomplete mobility matrices are a result of the current technological limitations for measuring rotational mobilities at a point. However, methods are available for estimating these mobilities when they are deemed important.

The synthesis results for the plate and equipment show similar shifts in resonance frequency locations and amplitudes relative to the experimental results for the combined structures. Differences in the results have been attributed to limitations of the experimental characterization of the equipment. The large data requirements of this method may be a limiting factor when trying to predict the coupled response of entire surfaces, which is required for radiated sound predictions. For components with small surface areas or applications requiring only a few FRFs (such as loss factor predictions), the large data requirements may not be an issue.

5 References

1. D'Ambrogio, W., Sestieri, A., "Substructure Coupling Using FRFS: Strategies for Tackling Rotational Degrees of Freedom," International Conference on Structural Dynamics Modeling, Portugal, 3-5 June, 2002.
2. Ewins, D. J., Modal Testing: Theory and Practice. John Wiley & Sons Incorporated, New York, NY, 1995.
3. Jetmundsen, B., Bielawa, R. L., Flannelly, W. G., "Generalized Frequency Domain Substructure Synthesis," *Journal of the American Helicopter Society*, 1988, pp. 55-64.
4. ABAQUS/Standard User's Manual, Volume 1, Version 5.6, 1996.
5. Gordis, J. H., Bielawa, R. L., and Flannelly, W. G., "A General Theory for Frequency Domain Structural Synthesis," *Journal of Sound and Vibration*, **150**(1), 1991, pp. 139-158.
6. Avitabile, P., "Twenty Years of Structural Dynamic Modification – A Review," *Journal of Sound and Vibration*, **73**(1), 2002, pp. 14-27.
7. MSC/Nastran 2001 user's manual, MSC Software corporation.
8. Munro, A. D., and Hambric, S. A., "Modeling Folded Beam Waveguide Absorber Behavior Using Translational and Rotational Degree of Freedom Frequency Response Function Coupling," *Proceedings of NOISE-CON 2003*, Cleveland, OH, June 2003.
9. Duarte, M. M., Ewins, D. J., "Rotational Degrees of Freedom for Structural Coupling Analysis via Finite-Difference Technique with Residual Compensation," *Mechanical Systems and Signal Processing*, **14**(2), 2000, pp. 205-227.
10. ANSI S2.34-1984, "American National Standard: Guide to the Experimental Determination of Rotational Mobility Properties and the Complete Mobility Matrix." Acoustical Society of America, New York.
11. Campbell, R. L., and Hambric, S. A., "Effects of Equipment Loading on The Vibrations of Edge-Stiffened Plates and Associated Modeling Issues," *Proceedings of 2002 ASME International Mechanical Engineering Congress and Exposition*, November 17-22, 2002, New Orleans, LA.